Waveguide-coupled micro-ball lens array suitable for mass fabrication

Lantian Chang,[1,2,*] Meindert Dijkstra,[3] Nur Ismail,[4] Markus Pollnau,[4] René M. de Ridder,[5] Kerstin Wörhoff,[6] Vinod Subramaniam,[1,2,7] and Johannes S. Kanger[1,2]

[1]*Nanobiophysics, MESA + Institute for Nanotechnology, University of Twente, 7500 AE Enschede, The Netherlands*
[2]*MIRA Institute for Biomedical Technology and Technical Medicine, University of Twente, 7500 AE Enschede, The Netherlands*
[3]*Optical Sciences Group, MESA + Institute for Nanotechnology, University of Twente, 7500 AE Enschede, The Netherlands*
[4]*Department of Materials and Nano Physics, School of Information and Communication Technology, KTH - Royal Institute of Technology, Isafjordsgatan, 22, SE-164 40 Kista, Sweden*
[5]*Faculty of Electrical Engineering, Mathematics and Computer Science, University of Twente, 7500 AE Enschede, The Netherlands*
[6]*LioniX BV, 7500 AL Enschede, The Netherlands*
[7]*FOM Institute AMOLF, Science Park 104, 1098 XG Amsterdam, The Netherlands*
**l.chang@utwente.nl*

Abstract: We demonstrate a fabrication procedure for the direct integration of micro-ball lenses on planar integrated optical channel waveguide chips with the aim to reduce the divergence of light that arises from the waveguide in both horizontal and vertical directions. Fabrication of the lenses is based on photoresist reflow which is a procedure that allows for the use of photolithography for careful alignment of the lenses with respect to the waveguides and enables mass production. We present in detail the design and fabrication procedures. Optical characterization of the fabricated micro-ball lenses demonstrates a good performance in terms of beam-size reduction and beam shape. The beam half divergence angle of 1544 nm light is reduced from 12.4 ° to 1.85 °.

OCIS codes: (130.0130) Integrated optics; (130.3120) Integrated optics devices; (130.3990) Micro-optical devices.

References and links

1. B. I. Akca, B. Považay, A. Alex, K. Wörhoff, R. M. de Ridder, W. Drexler, and M. Pollnau, "Miniature spectrometer and beam splitter for an optical coherence tomography on a silicon chip," Opt. Express **21**(14), 16648–16656 (2013).
2. G. Yurtsever, N. Weiss, J. Kalkman, T. G. van Leeuwen, and R. Baets, "Ultra-compact silicon photonic integrated interferometer for swept-source optical coherence tomography," Opt. Lett. **39**(17), 5228–5231 (2014).
3. N. Ismail, L. P. Choo-Smith, K. Wörhoff, A. Driessen, A. C. Baclig, P. J. Caspers, G. J. Puppels, R. M. de Ridder, and M. Pollnau, "Raman spectroscopy with an integrated arrayed-waveguide grating," Opt. Lett. **36**(23), 4629–4631 (2011).
4. C. L. Wei, F. Groen, M. K. Smit, I. Moerman, P. VanDaele, and R. Baets, "Integrated optical elliptic couplers: modeling, design, and applications," J. Lightwave Technol. **15**(5), 906–912 (1997).
5. N. Ismail, B. I. Akca, F. Sun, K. Wörhoff, R. M. de Ridder, M. Pollnau, and A. Driessen, "Integrated approach to laser delivery and confocal signal detection," Opt. Lett. **35**(16), 2741–2743 (2010).
6. C. Gmachl, "Plasmonics - a sharper approach," Nat. Photonics **2**(9), 524–525 (2008).
7. O. Mitomi, K. Kasaya, and H. Miyazawa, "Design of a single-mode tapered waveguide for low-loss chip-to-fiber coupling," IEEE J. Quantum Electron. **30**(8), 1787–1793 (1994).
8. F. Van Laere, T. Claes, J. Schrauwen, S. Scheerlinck, W. Bogaerts, D. Taillaert, L. O'Faolain, D. Van Thourhout, and R. Baets, "Compact focusing grating couplers for silicon-on-insulator integrated circuits," IEEE Photonics Technol. Lett. **19**(23), 1919–1921 (2007).
9. Y. M. Cheung and C. H. Yiu, "Simulation of the alignment sensitivity on the coupling efficiency of a ball-lens capped TO-Can laser diode source into a single-mode fiber," in *Proceedings of the 4th International Symposium on Electronic Materials and Packaging* (IEEE, 2002), pp. 197–203.

#243017 Received 17 Jun 2015; revised 28 Jul 2015; accepted 3 Aug 2015; published 17 Aug 2015

10. R. P. Ratowsky, L. Yang, R. J. Deri, K. W. Chang, J. S. Kallman, and G. Trott, "Laser diode to single-mode fiber ball lens coupling efficiency: full-wave calculation and measurements," Appl. Opt. **36**(15), 3435–3438 (1997).
11. R. G. Wilson, "Ball-lens coupling efficiency for laser-diode to single-mode fiber: comparison of independent studies by distinct methods," Appl. Opt. **37**(15), 3201–3205 (1998).
12. S. C. Shen and J. C. Huang, "Rapid fabrication of a micro-ball lens array by extrusion for optical fiber applications," Opt. Express **17**(15), 13122–13127 (2009).
13. C. H. Chien, C. T. Pan, C. C. Hsieh, C. M. Yang, and K. L. Sher, "A study of the geometry of microball lens arrays using the novel batch-fabrication technique," Sens. Actuators A Phys. **122**(1), 55–63 (2005).
14. MicroChemicals, "thick resist processing," http://www.microchemicals.com/technical_information/thick_resist_processing.pdf, Accessed 01–04–2015, 2015.
15. K. Wörhoff, P. V. Lambek, and A. Driessen, "Design, tolerance analysis, and fabrication of silicon oxynitride based planar optical waveguides for communication devices," J. Lightwave Technol. **17**(8), 1401–1407 (1999).
16. O. P. Lehar, M. A. Spak, S. Meyer, R. R. Dammel, C. J. Brodsky, and C. G. Willson, "Resist rehydration during thick film processing," Proc. SPIE **4345**, 463–474 (2001).
17. R. Diazuribe, M. Roseteaguilar, and R. Ortegamartinez, "Position sensing of a Gaussian-beam with a power-meter and a knife edge," Rev. Mex. Fis. **39**(3), 484–492 (1993).
18. O. Svelto, *Principles of Lasers,* 4th ed. (Springer, 2010).

1. Introduction

Light coupling between an integrated optical chip and free space is an important aspect in many applications. Typical waveguide systems have a mode size on the order of 1−3 μm, acting as very tight apertures at the end facets of the waveguide where the light is coupled out of the chip. These small apertures lead to strong divergence, on the order of tens of degrees, of the out-coupled beam. However, many applications require a collimated or focused light beam. Examples are on-chip optical coherence tomography (OCT) [1,2] and Raman spectroscopy [3]. A widely exploited approach is the use of one or more objective lenses to collimate or focus the light that emerges from the waveguide. However, the use of external lenses leads to a bulky setup requiring careful alignment, which would void the key advantages of using integrated optical chips. Therefore, an on-chip solution is preferred. Wei *et al.* demonstrated the use of a planar elliptic coupler at the end of a waveguide to focus the exit light in the horizontal direction [4]. Ismail *et al.* modified an arrayed waveguide grating for light delivery to, and light collection from a focal point in the horizontal direction [5]. Gmachl *et al.* demonstrated a reduction in vertical divergence using the surface-plasmon effect by fabricating a vertical gold grating at the end facet of a quantum-cascade laser cavity [6]. A drawback of all these methods is that they only reduce the divergence in one of the two lateral directions.

A major improvement would be an integrated solution to shape the exiting beam in both horizontal and vertical directions. A tapered waveguide or inverse-tapered coupler can enlarge the mode diameter to reduce the divergence angle in both directions [7]. However, it is technologically challenging to fabricate a vertical taper or a sharp inverse taper. Linear tapers do not allow focusing the light, and the fabrication of nonlinear vertical tapers poses additional difficulties. Focusing grating couplers can couple the light out of the wafer plane, which is very useful for wafer-scale testing [8]. However, gratings have inherent spectral limitations, especially in a low-refractive-index-contrast waveguide technology, making them less suitable for broadband applications. For example, a wavelength-insensitive solution will be preferred for applications like OCT, which require a broad wavelength range to achieve excellent in-depth resolution.

In this study, we demonstrate a method that accomplishes two-dimensional, wavelength-tolerant collimation or focusing of light coupled out of high-numerical-aperture channel waveguides by integrating micrometer-sized ball lenses with the optical waveguide chip. In the field of optical communication, commercially available ball lenses are used to realize efficient fiber-to-fiber or waveguide-to-fiber coupling [9–11]. In these studies, the ball lenses need to be aligned one by one, which is a precise and time consuming task. There are several

#243017 Received 17 Jun 2015; revised 28 Jul 2015; accepted 3 Aug 2015; published 17 Aug 2015

studies on the fabrication of on-chip micro-ball lens arrays, using a variety of approaches, which could reduce the alignment issue [12,13]. Our approach allows the integration of ball-lens fabrication with the fabrication of the waveguide structures, thus making the procedure suitable for mass production. Precise photolithographic alignment enables accurate positioning of all micro-ball lenses with respect to the optical waveguides.

We describe a process for fabricating polymeric micro-ball lenses that are aligned to silicon oxynitride (SiON) waveguides with silicon dioxide (SiO_2) cladding layers, on a silicon (Si) substrate. Design, fabrication, and characterization of a microlens array for application in an on-chip OCT system are discussed.

2. Design

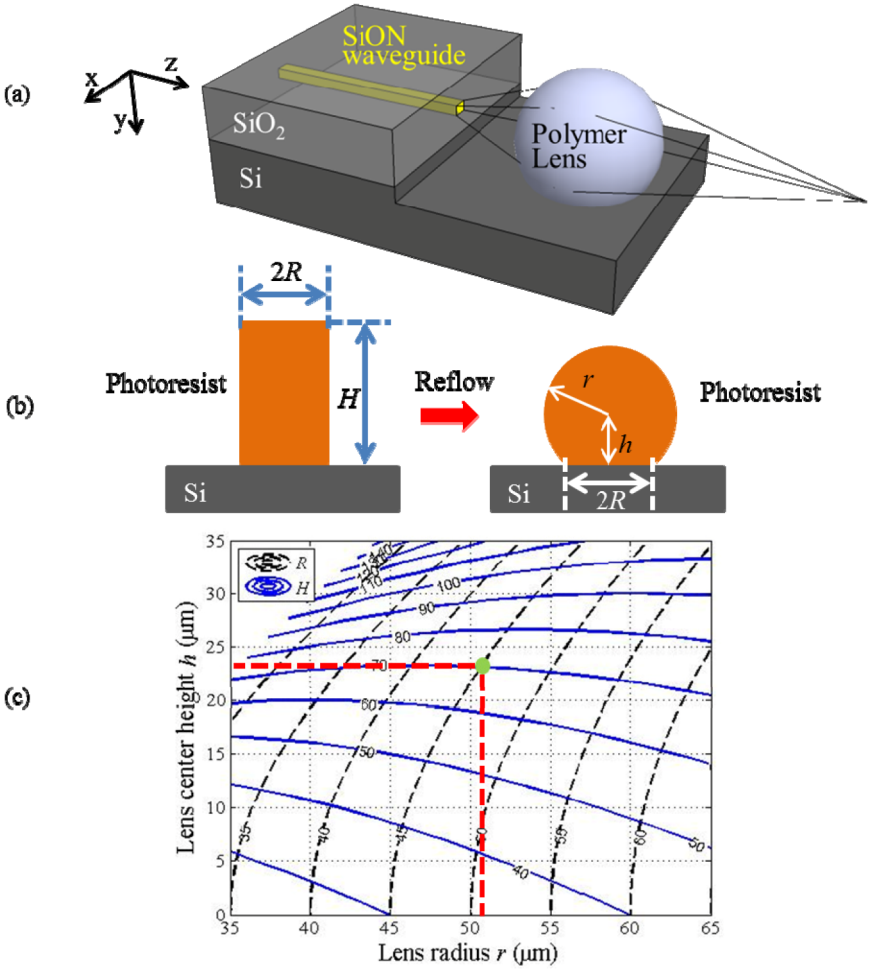

Fig. 1. (a) Schematic layout of a micro-ball lens integrated onto a SiON channel waveguide chip. (b) Schematic cross-section of the photoresist cylinder and its reflowed structure. (c) Diagram allows determining cylinder radius R (thin black dashed curves) and height H (thin blue solid curves) for a desired lens radius r and center height h. The thick dashed red lines show that a lens with r = 51 μm, h = 23 μm is obtained from a cylinder with R ≈45 μm, H ≈70 μm.

Figure 1(a) shows a schematic of the micro-ball lens integrated onto a SiON channel waveguide chip. The basic idea is to form a micro-ball lens by reflowing a photoresist cylinder. In this design, two masks (corresponding to two major fabrication steps) are needed

#243017 Received 17 Jun 2015; revised 28 Jul 2015; accepted 3 Aug 2015; published 17 Aug 2015

to integrate the micro-ball lenses with a given waveguide chip. The first major step is etching a platform through the SiO_2 cladding layer and into the Si substrate, in front of the waveguides. This lowered platform allows the vertical alignment of the micro-ball lens center to the waveguide facet. After depositing a photoresist layer of appropriate thickness, the second major step is patterning cylinders into the photoresist, which, after thermal treatment, will result in a reflowed spherically shaped microlens structure. The details of each fabrication step are described in the fabrication process section.

Figure 1(b) shows the geometrical dimension of a photoresist cylinder before the reflow and the micro-ball lens after the reflow. The radius r and center height h of the micro-ball lens are determined by the thickness H of the photoresist layer and the radius R of the patterned cylinder. The geometric model of the micro-ball lens is based on two assumptions. Firstly, the volume of the photoresist does not change during reflow. Secondly, the contact area of the Si substrate and the photoresist remains constant, due to the pinning effect provided by hexamethyldisilazane (HMDS) adhesion layer between the photoresist and Si. Given these assumptions, the radius r and center height h of the lens can be calculated as a function of the initial cylinder height H and radius R.

The volume V of the photoresist in its form of a cylinder before reflow is given by:

$$V = V_{cylinder} = \pi R^2 H. \tag{1}$$

The same volume V of the photoresist in the form of a micro-ball lens after reflow can be calculated as:

$$V = V_{ball-lens} = \frac{2}{3}\pi r^3 + \pi r^2 h - \frac{1}{3}\pi h^3. \tag{2}$$

Because the radius R of the contact area is assumed to be constant, the following relation holds:

$$r^2 = h^2 + R^2. \tag{3}$$

The effective focal length f (distance between the ball center to the focal point) of a ball lens in air can be calculated with:

$$f = \frac{n}{2(n-1)} r, \tag{4}$$

where n is the refractive index of the photoresist, which in our case is equal to 1.59 at a wavelength of λ = 1550 nm.

Equations (1)-(3) are used to calculate the relationship between the cylinder height H, the cylinder radius R, the lens center height h, and the lens radius r. The calculated results are shown in Fig. 1(c). This graph allows one to determine the required dimensions of the cylinder (R, H) to achieve the target dimensions of the lens (r, h).

In order to fabricate appropriate lenses for a specific application, a set of design parameters can be obtained from the calculations above. The focal length f of the micro-ball lens should be determined by the mode shape of the waveguide and the desired beam shape after the lens. In our example, an f has been chosen around 69 μm to collimate the light from our waveguide to a beam close to 40 μm in diameter. From Eq. (4), the required lens radius r can be calculated as r = 51 μm. The clear aperture of the lens should be larger than the beam diameter in the lens to ensure a low distortion of the beam. The clear aperture of our micro-ball lens is limited by the lens center height h. In this example, h should be larger than half the beam diameter, which is 20 μm. Considering a Gaussian beam, there is energy outside of the $1/e^2$ beam radius and it is extended to infinity, thus, a larger h provides a better result.

#243017 Received 17 Jun 2015; revised 28 Jul 2015; accepted 3 Aug 2015; published 17 Aug 2015

Taking h = 23 μm and r = 51 μm as an example, Fig. 1(c) shows a required cylinder radius R ≈45 μm and height H ≈70 μm to produce the desired micro-ball lens.

Given a lens radius r, the center height h of the lens can, in principle, be chosen freely between a minimum value set by the aperture (20 μm) of the emerging beam at the position of the lens and a maximum value set by the lens radius r (51 μm). However, for increasing values of h, larger values for the cylinder height H are required. Given the fact [14] that the fabrication process becomes increasingly difficult for larger photoresist layer thicknesses H, the best choice for h would be close to the minimum value.

Depending on the application, the distance between the facet of the waveguide and the lens center can be arranged freely to achieve either a diverged, collimated, or focused beam behind the micro-ball lens. There are, however, limitations. On the one hand, because the lens should not touch the waveguide facet to avoid deformation of the shape of the lens during the reflow, it should not be placed too close to the waveguide facet. On the other hand, because it should be avoided that the diverging beam coming out from the waveguide hits the substrate and creates a mirror reflection from the substrate, the lens should not be placed too far from the waveguide facet.

3. Fabrication process flow

The process flow charts for etching the platform and fabricating the lens are shown in Figs. 2 and 3 respectively.

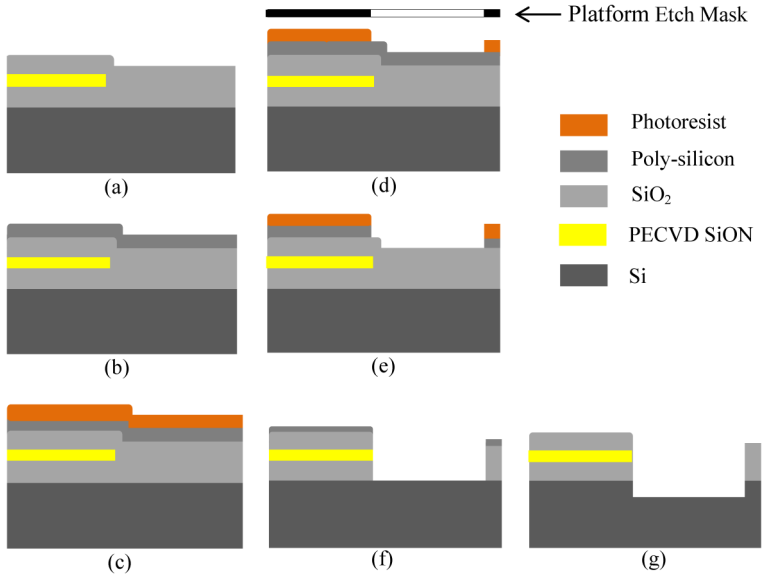

Fig. 2. Process flow chart for etching the platform on which the lenses are to be fabricated.

The starting point is 100-mm <100> silicon wafer with SiON channel waveguides as shown in Fig. 2(a). The applied SiON waveguide technology was developed in the Integrated Optical MicroSystems group at the University of Twente [15]. The waveguides are fabricated on an 8 μm thick thermal SiO_2 layer. The waveguide core [yellow layer in Fig. 2(a)] is a 600 nm thick, 2 μm wide SiON layer with a refractive index of 1.547 at λ = 1550 nm. This film is deposited by plasma-enhanced chemical vapor deposition (PECVD), followed by a thermal annealing step for 3 hours at 1100°C. The channel waveguides are fabricated by standard lithography in combination with reactive ion etching (RIE) utilizing a CHF_3/ O_2 chemistry. The top cladding is composed by a 1 μm thick SiO_2 layer, grown by low-pressure chemical

#243017 Received 17 Jun 2015; revised 28 Jul 2015; accepted 3 Aug 2015; published 17 Aug 2015

vapor deposition (LPCVD) using tetraethyl orthosilicate (TEOS) and a 3 µm thick PECVD SiO_2 layer. Following the deposition steps the films are annealed at 1100°C.

On top of the top cladding, a 1.1 µm thick LPCVD poly-silicon layer is grown [dark grey layer in Fig. 2(b)]. This layer is applied as a hard mask during the deep SiO_2 etching.

In order to pattern the poly-silicon mask, a 1.7 µm thick positive photoresist (Olin OiR 907-17) layer is spin coated (4000 rpm, 30 s) on top of the poly-silicon layer [orange layer in Fig. 2(c)] and then patterned with the platform etch mask. The resulting cross section is schematically shown in Fig. 2(d).

Then the poly-silicon layer is dry-etched for 50 seconds in a Tetske machine by an SF_6-based RIE process. The schematic etch result is shown in Fig. 2(e). The etch rate of the applied RIE recipe strongly depends on the etch "load", i.e., the required etching time has a negative correlation to the area covered with photoresist.

The 12 µm thick SiO_2 stack is etched for 27 min. in an Adixen AMS 100 DE machine, and all of the photoresist 907-17 layer and most of the poly-silicon layer is etched away as shown in Fig. 2(f). Thereafter the silicon is etched by a Bosch standard high aspect ratio silicon etch recipe (B-HARS) in an Adixen AMS 100 SE machine. In this step the remaining poly-silicon is removed and the platform pattern is etched into the silicon wafer to a depth of 16 µm [as indicated in Fig. 2(g)]. The load dependence of this recipe results in an etching procedure which is separated into two stages. The first stage is a slow etching stage. The remaining poly-silicon layer together with the exposed Si substrate in the platform results in a 100% load, which leads to a very slow etch rate (< 1 µm/min). The second stage starts as soon as the poly-silicon layer has been etched away. For our design the etch load is reduced to 1%. Consequently the etch rate of the silicon substrate increases to 4 µm/min. The height difference between the center of the waveguide and the bottom of the platform is 24 µm, which corresponds approximately to the desired center height of the micro-ball lens.

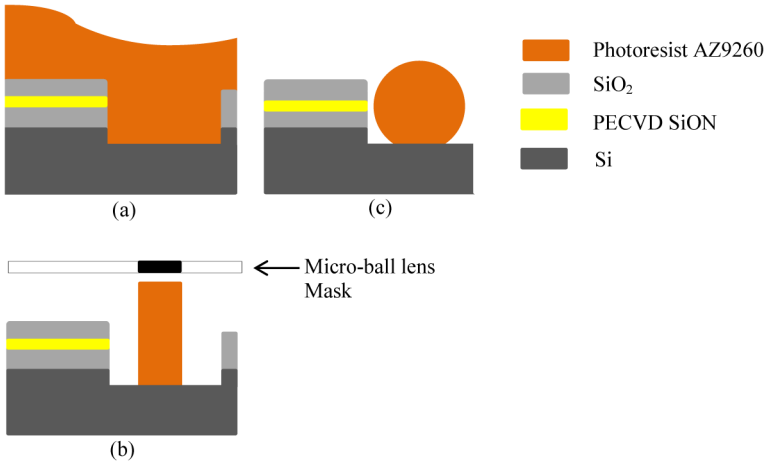

Fig. 3. Process flow chart for the fabrication of a photo-definable micro-ball lens array aligned to the channel waveguides.

The process flow chart of the photoresist micro-ball lens fabrication is shown in Fig. 3. The selected photoresist should fulfill the following requirements: reflowable to form a ball shape; low losses in the wavelength range of interest; suitable for the fabrication of a thick layer (70 µm thickness in our case). AZ9260 is one of the photoresists that fulfill all three requirements. For adhesion improvement vapor phase HMDS treatment was applied to the wafers prior to resist coating. By two AZ9260 coating and several baking steps, the thick photoresist layer as shown in Fig. 3(a) is produced. This double layer coating procedure results in a photoresist thickness of 72 µm inside the platform.

#243017 Received 17 Jun 2015; revised 28 Jul 2015; accepted 3 Aug 2015; published 17 Aug 2015

For the patterning of the photoresist layer a photolithographic process is needed in which water molecules play an essential role during the exposure [16]. The AZ9260 is a diazonaphthoquinone-based resist, and its primary ketene photoproduct can react rapidly with water molecules to form a dissolution promoter, which will make the exposed resist soluble in the developer. However, if no water molecules are present, a slower reaction between the ketene photoproduct and the Novolak matrix [16] becomes dominant. This slower reaction produces an inhibitor which causes the exposed resist to become insoluble in the developer. During the baking steps water has been effectively removed from the resist layer. Therefore, rehydration in a humid environment is needed prior to exposure. Since the rehydration process relies on diffusion of the water molecules, the rehydration time is proportional to the square of the resist layer thickness. For a 70 μm thick layer, a typical rehydration time in a 100% relative humidity environment (20 °C) is about 20 hours. A faster alternative way to rehydrate the resist layer is water immersion, which has been demonstrated by Lehar *et al.* [16]. It was found that sufficient rehydration in our resist layer is obtained by immersing the wafer into 30 °C water for 15 min., followed by 3.5 hours in a cleanroom environment (20 °C, 48% relative humidity). This reduction in process time can be attractive for mass production. The rehydrated resist film is exposed in an EV620 Mask Aligner at a dose of 3 J/cm^2. Subsequently, the resist is developed in the developer OPD4262 for 40 minutes. The schematic result after developing is shown in Fig. 3(b). The reflow of AZ9260 is performed on a 120 °C hot plate for 2 minutes. Finally, the wafer is diced in order to bring the lens array close to the chip edge, as shown in Fig. 3(c).

4. Fabrication results

Hundreds of micro-ball lenses were fabricated on three wafers. The yield (good shape and location by visual observation using a microscope) is above 95% before dicing and reduced to 85% after dicing. Most common failures are lenses with bubbles or lenses missing. During the dicing process, 10% of the micro-ball lenses are lost or damaged by the constant cooling water jet of the dicing blade. To improve the overall yield, a dry dicing or cleaving machine is preferred.

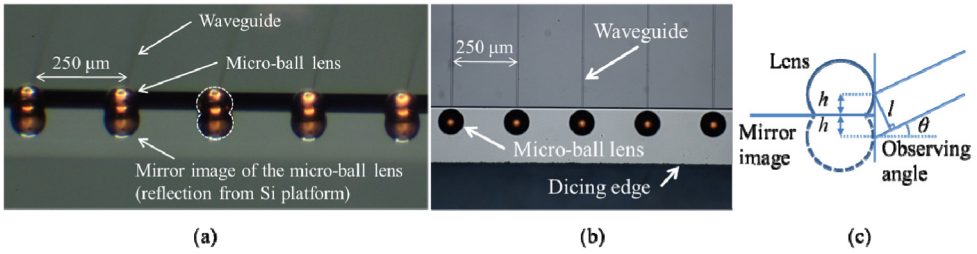

Fig. 4. (a) Bird's-eye view of a fabricated micro-ball lens array before dicing the chip. There are 5 waveguides at 250 μm spacing in this image. The outline of the middle lens and its mirror image has been drawn to guide the eye. (b) Top view of a micro-ball lens array after dicing. (c) Geometry layout used to calculate the lens center height $h = l / (2\cos(\theta))$ from the observed distance l and observing angle θ.

Fabricated micro-ball lenses and waveguides are shown in Fig. 4. A bird's-eye view of a lens array before dicing is shown in Fig. 4(a). There is one micro-ball lens in front of each waveguide. The silicon surface of the platform is smooth enough to show clear mirror images of the lenses. A top view of the same micro-ball lens array after dicing is shown in Fig. 4(b). All the lenses are well aligned in front of each waveguide. The dicing edge is about 100 μm from the lens edge. The lens radius $r = 49 \pm 1$ μm is measured from the top-view image. The lens center height $h = l / (2\cos(\theta)) = 24 \pm 1\,\mu\text{m}$ is measured indirectly from the bird's-eye-view image by knowing the bitangent line segment length l [as indicated in Fig. 4(c)] of the lens

#243017 Received 17 Jun 2015; revised 28 Jul 2015; accepted 3 Aug 2015; published 17 Aug 2015

and its mirror image outline, as well as the angle θ of view of the image with respect to the wafer plane. The dimensions of all lenses are identical within the measurement accuracy and are in good agreement with the calculation based on Fig. 1(c).

The horizontal lens-waveguide alignment accuracy is limited by the lithographic process. In our case, the maximum inaccuracy is specified as 1 µm. Measurements on a few samples showed the actual misalignment error to be 0.7 ± 0.2 µm. The vertical lens-waveguide alignment can be controlled with accuracy of 1 µm for the ball lens size we used. The main contribution to the vertical alignment error is the cylinder height before reflow. We believe that the uncertainty introduced by our current manual double-coating procedure can be considerably reduced by using an automated photoresist spin coating machine.

To test the mechanical stability of the lenses, destructive experiments were performed with a Nordson Dage 4000Plus Bondtester. The measured average force to destroy/remove a micro-ball lens by pushing from the side is 6 centinewton (cN) with a standard deviation of 1.5 cN. A micro-ball lens has a mass on the order of 10^{-6} g, which means the lens should be able to withstand an acceleration in the order of 10^{7} m/s^2. This indicates a good mechanical stability of the lenses.

5. Optical characterization and discussion

In order to measure the optical performance of the micro-ball lenses, beam profiles behind the micro-ball lenses were measured with a home-built knife-edge setup at a wavelength of 1544 nm. An example of a measurement is shown in Fig. 5. In this particular measurement, the knife edge is 1.2 mm away from the waveguide end.

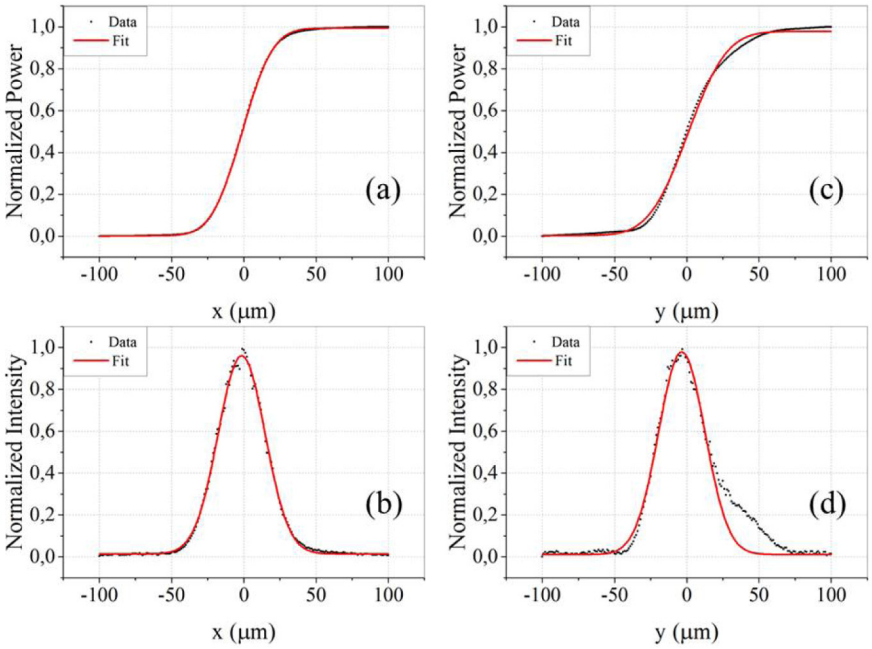

Fig. 5. Beam profile (at λ = 1544 nm) behind a micro-ball lens measured with a knife-edge setup at 1.2 mm away from the waveguide end. (a) and (c) display the measured power and their fitting in the horizontal (x) and vertical (y) direction, respectively. (b) and (d) display the derivative of the measured data and its Gaussian fitting of (a) and (c), respectively.

Figure 5(a) shows the normalized power as measured during one knife-edge scan in the x direction (parallel to the chip dicing edge). The data is fitted using the following expression [17] for the measured power P, which assumes a Gaussian intensity profile of the beam:

#243017 Received 17 Jun 2015; revised 28 Jul 2015; accepted 3 Aug 2015; published 17 Aug 2015

$$P = P_0 + \frac{P_{\max}}{2}\,\mathrm{erf}\left(\frac{\sqrt{2}\,(x - x_0)}{w}\right), \tag{5}$$

with P_0, the background power, P_{max}, the maximum power, x_0 the center position of the Gaussian intensity profile, and *erf* is a standard error function. The $1/e^2$ beam radius w is obtained by the fitting procedure. The result of this fit is shown in Fig. 5(a). The x derivative of the measured power P yields the intensity profile in the x direction as shown in Fig. 5(b). In Figs. 5(c) and 5(d), the power and intensity profile in the y direction (perpendicular to the chip plane) are shown. The positive y direction in this case is defined from the lens center point down to the Si substrate. The values for the beam radius w in x and y directions as obtained from the fit are 32.4 μm and 32.1 μm, respectively.

It can be observed from Figs. 5(b) and 5(d) that the beam shape in the x direction fits much better to a Gaussian-shaped beam profile compared to the y direction. In the y direction, the lower part of the beam (at positive values for y) deviates from a Gaussian shape. This is due to the fact that the Gaussian beam has a tail extending to infinity and its lower part (outside the e^{-2} beam radius, where the intensity is not yet negligible) is disturbed by the bottom of the truncated lens. Diffraction of the disturbed Gaussian beam results in the observed extended tail in the y direction.

For some applications, a better beam shape may be needed. In that case, the platform should be etched a few micrometers deeper and the micro-ball lens center should be elevated by the same amount to reduce blocking of the Gaussian tail by the platform.

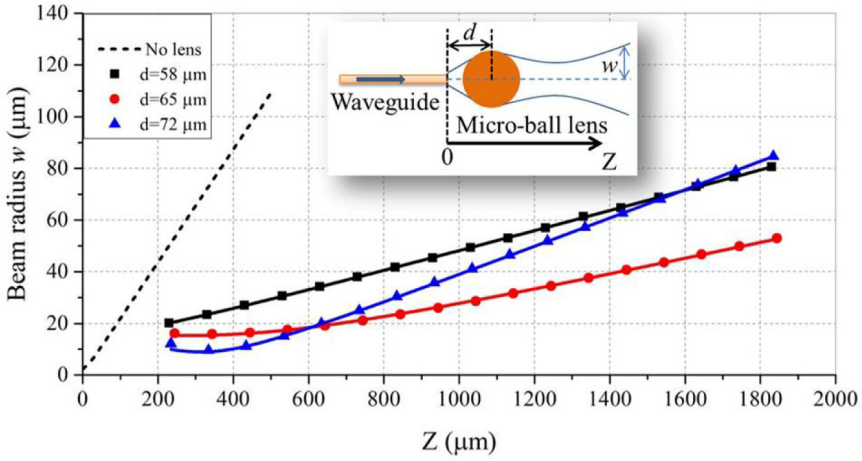

Fig. 6. Beam radius ($1/e^2$ radius) measurements in x direction for different waveguide-lens distances with a knife-edge setup. z is the beam propagation direction and z = 0 is the end facet of the waveguide. The distance between the waveguide end facet and the lens center is d. The dashed line is the simulated beam size from a waveguide without a micro-ball lens. The half divergence angle of this beam is 12.4 degree. The black, red, and blue lines are the fitted results of the measurements with d equal to 58 μm, 65 μm, and 72 μm, respectively.

To further analyze the optical performance of the lens, the beam radius $w(z)$ along the x direction was measured at different positions z along the optical axis for three different structures at a wavelength of 1544 nm using the knife-edge method (Fig. 6). The data are fitted to the beam radius expected for a Gaussian beam as given by [17]:

$$w(z) = w_0\sqrt{1 + \frac{(z - z_0)^2}{z_R}};\ \text{with}\ z_R = \frac{\pi w_0^2}{\lambda}, \tag{6}$$

#243017 Received 17 Jun 2015; revised 28 Jul 2015; accepted 3 Aug 2015; published 17 Aug 2015

where z_0 is the position of the beam waist w_0, λ is the wavelength (1544 nm), and z_R is the Rayleigh range. Fitting the data using Eq. (6) yields the size w_0 and location z_0 of the beam waist. The fit results for all three structures are good, confirming our earlier conclusion based on Fig. 5(b) that the beam profile along the x direction is well approximated by a Gaussian distribution. The extended tail in the y direction changes shape and position as a function of location z which lead to a difficultly to accurately determine the beam radius $w(z)$ at all locations z. However, the main peak has similar beam radius in both x and y direction as shown in Figs. 5(b) and 5(d). Therefore, simple Gaussian beam parameters can be used to approximate the behavior of the beams. In this case the far-field half-divergence angles θ can be calculated using [18]:

$$\tan(\theta) = \frac{\lambda}{\pi w_0}. \tag{7}$$

With the micro-ball lenses placed at d = 58 μm, d = 65 μm, and d = 72 μm, the obtained far-field half-divergence angles are 2.28 °, 1.85 °, and 3.17 °, respectively. To compare these results to the case in which no micro-ball lens is used, Fig. 6 shows also a calculated beam radius for the case where the beam is coupled out from the waveguide without a micro-ball lens. In this case, the half-divergence angle is 12.4 degree. The divergence of this beam is so large that the beam size is larger than our knife-edge detector at the shortest possible measurement distance, and as such no accurate measurement of this beam could be performed.

The experimental results shown in Figs. 5 and 6 demonstrate that the micro-ball lens can strongly reduce the divergence angle of light emerging from a waveguide in both horizontal and vertical directions. Obviously, the beam divergence can be varied within certain limits by changing the distance between the lens and the waveguide end facet in the mask design.

The optical loss of the micro-ball lens is simulated to be 11% at the wavelength of 1544 nm. Preliminary loss measurements have been performed. Limitations of the current measurement system, allowed only the estimation of an upper limit of 20% for the insertion loss. Further study into this issue is planned.

6. Conclusion

In this study, we have demonstrated an integrated micro-ball lens system that allows for a significant reduction of the divergence angle of a light beam radiated from the end facet of an optical chip in both horizontal and vertical direction. The fabrication procedure allows careful tuning of the physical dimensions of the lens. In principle, the fabrication procedure is suitable for mass production, however the current yield of 85% needs to be improved. Furthermore, the fabrication strategy is not limited to the SiON waveguide platform as used here. It can be anticipated that, by carefully choosing suitable etching recipes for the fabrication of the platform and the right adhesion material in between the photoresist and the substrate, the strategy described here can be applied to waveguide technologies that are based on other materials.

Acknowledgments

The authors acknowledge support from the IOP Photonic Devices program (Low-cost handheld OCT device, IOP PD100019) managed by the Technology Foundation STW and RVO.

#243017 Received 17 Jun 2015; revised 28 Jul 2015; accepted 3 Aug 2015; published 17 Aug 2015